

Automatic detection of full ring galaxy candidates in SDSS

Lior Shamir,¹★

¹*Kansas State University, Manhattan, KS 65506, USA*

Accepted XXX. Received YYY; in original form ZZZ

ABSTRACT

A full ring is a form of galaxy morphology that is not associated with a specific stage on the Hubble sequence. Digital sky surveys can collect many millions of galaxy images, and therefore even rare forms of galaxies are expected to be present in relatively large numbers in image databases created by digital sky surveys. Sloan Digital Sky Survey (SDSS) data release (DR) 14 contains $\sim 2.6 \cdot 10^6$ objects with spectra identified as galaxies. The method described in this paper applied automatic detection to identify a set of 443 ring galaxy candidates, 104 of them were already included in the Buta + 17 catalogue of ring galaxies in SDSS, but the majority of the galaxies are not included in previous catalogues. Machine analysis cannot yet match the superior pattern recognition abilities of the human brain, and even a small false positive rate makes automatic analysis impractical when scanning through millions of galaxies. Reducing the false positive rate also increases the true negative rate, and therefore the catalogue of ring galaxy candidates is not exhaustive. However, due to its clear advantage in speed, it can provide a large collection of galaxies that can be used for follow-up observations of objects with ring morphology.

Key words: Catalogs — techniques: image processing — methods: data analysis — galaxies: peculiar

1 INTRODUCTION

The deployment of autonomous digital sky surveys has enabled the creation of very large databases of galaxy images, and therefore even very rare types of galaxies are assumed to be present in these databases. One of the less common types of galaxies is ring galaxies. Ring galaxies can be separated into several different types (Buta & Combes 1996) such as bar-driven or tidially-driven resonance rings (Buta 2000), collisional rings (Appleton & Struck-Marcell 1996), polar rings (Whitmore et al. 1990; Macciò et al. 2005; Reshetnikov & Sotnikova 1997; Finkelman et al. 2012; Reshetnikov & Combes 2015), “Hoag-type” rings (Hoag 1950; Brosch 1985; Schweizer et al. 1987), and spiral galaxies with ringed bars (Buta et al. 2001).

Ring galaxies can be classified by their visual morphology into three major sub-classes (Theys & Spiegel 1976): Empty rings (RE), rings with off-centre nucleolus (RN), and rings with knots or condensations (RK). Another classification scheme for ring galaxies based on their visual appearance separates ring galaxies into “O-rings”, which have a smooth ring structure and a nucleolus in its centre, and “P-type” rings, which have a knotty structure or a nucleolus that is not in the centre of the ring (Few & Madore 1986).

Some ring galaxy catalogues were created using manual analysis of the galaxies in the past six decades. The catalogue of peculiar galaxies of Arp (1966) includes two empty ring galaxies, and the Arp & Madore (1988) catalogue includes 69 ring galaxies. Struck (2010) prepared a catalogue of a dozen colliding ring galaxies from SDSS based on reports of volunteers in the Galaxy Zoo on-line forum. The Whitmore et al. (1990) catalogue included 157 polar ring galaxy candidates, and several of these galaxies were confirmed as polar rings (Finkelman et al. 2012). Madore et al. (2009) released an atlas of collisional rings. Garcia-Ribera et al. (2015) identified 16 polar ring galaxy candidates. Buta (1995) collected a set of Southern ring galaxies. Moiseev et al. (2011) and (Buta 2017) used citizen science annotations and classifications to identify ring galaxy candidates by using the Galaxy Zoo 1 and Galaxy Zoo 2 databases, respectively. These catalogues are efficient in the sense that they have good detection accuracy due to the superior ability of the human brain to analyze galaxy morphology, but because they require very intensive labour, even when using a large number of volunteers it is difficult to perform an exhaustive analysis of the entire image databases collected by modern digital sky surveys. That bandwidth limitation will be magnified when more powerful sky surveys such as LSST see first light. Timmis & Shamir (2017) used computer analysis to release a

★ E-mail: lshamir@mtu.edu

catalogue of 186 automatically identified ring galaxy candidates in PanSTARRS.

As digital sky surveys become increasingly more powerful, it is clear that manual analysis of the images is not sufficient for comprehensive detection of ring galaxies among millions of galaxy images. That reinforces the use of automation to detect ring galaxies. The ability to identify galaxy morphology automatically can lead to much larger collections of ring galaxies, which can also be useful when more powerful digital sky surveys such as LSST start to collect data.

2 GALAXY IMAGE ANALYSIS METHOD

The data source used in this study is the set of galaxies with spectra in SDSS DR14. SDSS DR14 contains a total of $\sim 4.8 \cdot 10^6$ IDs of objects with spectra, and $\sim 2.6 \cdot 10^6$ of these objects are labeled by SDSS pipeline as galaxies. The mean redshift of these galaxies is 0.38 ($\sigma=0.24$), and the mean g magnitude is ~ 20.56 ($\sigma=2.09$). The image of each galaxy was obtained by using the *cutout* service of SDSS as was done in (Kuminski & Shamir 2016). In summary, the images are downloaded as 120×120 JPG colour images. Since galaxies have different sizes, each galaxy was downloaded several times until 25% or less of the pixels on the edges of the image have gray value of less than 125. The initial scale was set to 0.25" per pixel, and it increased by 0.05" until 25% or less of the pixels on the edges are not bright, which means that the galaxy fits inside the image (Kuminski & Shamir 2016).

The JPG images are used because they combine information from the different bands, providing a simple image format that contains information about the morphology of each object in a manner that is easier to process by machine vision. While the original FITS format allows to make accurate photometric measurements, that accuracy is not required for machine vision systems for the purpose of broad morphological analysis. Therefore, the simple JPG format provides an efficient mechanism for both manual (Willett et al. 2013) and automatic (Dieleman et al. 2015; Kuminski & Shamir 2016) analysis.

Downloading that large dataset of galaxy images required ~ 16 days. The image analysis method is similar to the method used in Timmis & Shamir (2017). Each image was converted to a binary map such that all pixels above the threshold were set to 1, and the pixels below the threshold were set to 0. The initial threshold was set to 50, and increased by five until it reached 200.

For each threshold, the image is inverted, and a 4-connected labeling algorithm is applied to label all objects in the inverted image. If more than one object is detected, it means that the image contained background areas that are inside foreground objects, and therefore could be rings. Since a galaxy can contain many small areas inside the arms, if the size of the background area is less than 10% of the foreground galaxy the algorithm ignores that background area and does not consider it as a ring candidate. The algorithm is implemented as part of the Ganalyzer galaxy image analysis tool (Shamir 2011a,b).

3 RING GALAXY CANDIDATES

The method described in Section 2 and also explained in (Timmis & Shamir 2017) detected ring galaxy candidates, as listed in Table 1. The galaxies are provided with their catalogue number, right ascension and declination of each object.

The images of the galaxies are shown by Figures 1, 2, 3, 4, and 5, showing candidate resonance ring galaxies, collisional rings, rings with an off-centre nucleus, rings with no obvious nucleus, and other rings, respectively.

No	RA ($^{\circ}$)	Dec ($^{\circ}$)	No	RA ($^{\circ}$)	Dec ($^{\circ}$)	No	RA ($^{\circ}$)	Dec ($^{\circ}$)	No	RA ($^{\circ}$)	Dec ($^{\circ}$)
1	249.478	45.695	2	146.776	54.312	3	204.487	-1.718	4	134.007	42.273
5	151.691	48.628	6	174.501	48.439	7	240.680	41.197	8	150.674	12.624
9	178.885	46.219	10	247.738	21.791	11	242.607	17.760	12	184.600	20.141
13	175.241	17.219	14	177.949	2.0095	15	151.699	-0.503	16	188.017	66.405
17	313.869	0.5356	18	147.504	47.108	19	254.346	25.465	20	246.945	38.943
21	345.459	0.8371	22	206.989	34.975	23	142.281	30.142	24	212.959	31.927
25	209.728	29.576	26	121.734	13.760	27	161.107	26.490	28	199.832	21.625
29	200.213	12.157	30	181.458	-0.184	31	114.872	32.724	32	130.460	45.426
33	344.860	15.151	34	32.5462	0.8323	35	191.767	51.582	36	169.010	52.136
37	134.635	37.087	38	196.905	49.771	39	157.796	6.8742	40	236.009	45.956
41	212.605	57.661	42	121.289	25.396	43	157.020	37.820	44	202.846	10.891
45	210.915	36.730	46	226.564	10.340	47	358.794	0.6218	48	45.2437	0.0599
49	115.312	47.646	50	153.830	11.924	51	182.373	39.815	52	185.316	36.335
53	212.079	29.079	54	196.828	31.078	55	219.011	26.653	56	232.845	20.023
57	216.339	25.179	58	246.557	13.215	59	185.591	29.581	60	195.454	19.008
61	125.013	11.941	62	126.532	10.747	63	132.706	11.309	64	21.8792	14.819
65	358.874	14.192	66	334.402	12.700	67	343.107	13.176	68	178.438	55.528
69	136.982	42.311	70	134.690	46.042	71	156.889	45.897	72	224.223	49.878
73	164.944	42.657	74	164.202	44.303	75	238.755	34.936	76	236.775	30.955
77	242.395	27.670	78	349.965	0.4225	79	323.714	0.3869	80	202.922	14.237
81	192.539	35.383	82	180.130	31.947	83	161.572	29.359	84	209.222	20.142
85	174.478	21.985	86	165.202	15.602	87	169.606	17.286	88	21.3182	-8.873
89	179.819	-1.108	90	57.4584	0.0522	91	211.549	-1.227	92	222.089	-0.807
93	173.951	-0.494	94	186.144	0.3766	95	27.7023	13.568	96	21.3422	14.838
97	56.1696	-5.625	98	172.324	-1.708	99	188.859	-3.602	100	131.250	52.393
101	121.762	45.676	102	198.947	-0.462	103	139.699	55.705	104	129.686	50.619
105	118.790	44.173	106	120.193	47.176	107	212.371	64.913	108	193.725	1.5910
109	232.049	2.5300	110	216.834	1.0258	111	200.184	1.7388	112	161.881	2.0791
113	148.000	2.5866	114	211.465	3.0833	115	211.105	3.7596	116	217.769	4.8296
117	337.496	-8.593	118	326.511	-7.198	119	330.341	-7.128	120	33.5925	-9.104
121	12.6542	-9.068	122	327.665	-8.332	123	310.736	-5.808	124	325.317	-7.257
125	344.334	14.366	126	349.625	14.826	127	3.76	-10.155	128	40.2084	-7.975
129	120.524	41.188	130	136.520	51.735	131	12.3798	15.987	132	148.945	1.6018
133	167.917	1.5236	134	172.665	1.5887	135	166.954	2.3566	136	143.045	55.219
137	149.479	4.2610	138	159.731	4.8516	139	154.457	-0.829	140	217.412	3.2662
141	216.152	4.5591	142	142.796	52.635	143	171.822	3.7559	144	245.442	43.355
145	198.781	62.521	146	154.892	60.226	147	199.446	61.082	148	227.381	54.506
149	223.241	56.502	150	235.794	1.3288	151	236.464	1.6150	152	254.836	32.164
153	247.893	40.565	154	247.611	41.483	155	254.044	34.836	156	202.138	-2.215
157	209.293	-2.121	158	210.519	-1.357	159	203.819	-2.556	160	218.867	-2.077
161	217.009	-1.851	162	217.181	-1.696	163	221.867	-1.633	164	258.276	33.319
165	219.552	-1.517	166	214.472	6.2075	167	331.913	11.623	168	327.669	12.683
169	344.061	12.884	170	319.137	10.165	171	322.616	11.734	172	313.865	-1.225
173	321.890	-1.188	174	337.481	-0.751	175	310.202	1.0436	176	348.231	-0.906
177	22.7615	0.6365	178	12.0399	-0.912	179	4.22992	-0.460	180	163.053	55.220
181	168.702	56.578	182	138.148	45.262	183	177.635	55.057	184	181.786	55.179
185	185.964	56.049	186	124.311	37.030	187	168.055	50.536	188	121.207	29.331
189	165.645	50.582	190	120.283	29.148	191	147.666	46.679	192	182.677	53.037
193	148.591	51.243	194	152.806	53.516	195	141.639	48.011	196	118.186	25.786
197	164.499	51.017	198	151.799	48.755	199	150.764	45.597	200	115.717	22.112
201	127.439	32.611	202	138.063	39.126	203	178.757	48.786	204	126.713	4.4197
205	149.480	55.911	206	172.044	60.538	207	176.594	6.8419	208	152.865	6.6629
209	170.926	7.5019	210	170.435	9.0033	211	172.277	8.9885	212	195.901	8.9922
213	197.627	9.0227	214	170.275	9.6956	215	143.277	8.1112	216	184.366	67.558
217	183.089	68.120	218	183.552	68.354	219	157.983	50.684	220	158.091	50.698
221	198.592	53.077	222	189.000	54.220	223	170.973	53.848	224	175.943	54.442
225	180.213	54.591	226	185.335	54.761	227	242.073	38.176	228	244.923	36.088
229	245.153	36.365	230	228.312	48.495	231	214.146	55.481	232	204.799	57.900
233	246.322	38.792	234	235.189	47.867	235	240.961	44.508	236	242.529	43.458
237	49.9495	-0.221	238	150.004	8.5004	239	152.192	9.1769	240	174.041	10.055
241	159.028	45.131	242	142.741	8.9121	243	133.555	6.9731	244	144.494	10.299
245	124.369	7.6804	246	143.128	11.715	247	170.282	15.133	248	128.269	27.860
249	143.547	33.935	250	226.157	40.372	251	157.685	40.057	252	231.672	46.582
253	242.420	39.406	254	251.975	32.123	255	222.494	52.609	256	211.155	54.793
257	213.933	54.043	258	211.272	43.273	259	195.093	47.445	260	218.954	42.539
261	213.271	44.608	262	205.493	46.874	263	163.419	42.012	264	165.450	44.449
265	190.911	44.094	266	173.248	43.993	267	178.491	44.535	268	209.072	12.177
269	215.581	47.935	270	204.184	51.544	271	168.958	41.409	272	190.235	42.905
273	173.123	42.806	274	166.485	6.3174	275	188.748	6.6979	276	175.650	7.0617
277	186.338	42.850	278	240.874	24.456	279	180.837	39.608	280	238.010	26.315
281	245.992	21.820	282	193.027	39.818	283	229.797	7.4837	284	200.312	8.5059
285	227.996	6.0962	286	213.297	8.4694	287	217.921	8.0661	288	229.609	5.2192
289	230.929	5.0401	290	227.691	6.3661	291	193.573	51.172	292	233.115	41.811
293	238.011	39.112	294	237.939	38.960	295	232.652	42.717	296	201.442	40.103
297	236.668	28.128	298	214.405	38.164	299	230.211	33.388	300	240.475	31.892
301	242.052	30.739	302	251.416	20.549	303	250.602	26.474	304	240.146	28.965
305	241.110	7.6260	306	243.344	7.0388	307	225.839	11.308	308	248.723	23.211
309	211.579	36.833	310	223.355	33.283	311	231.612	28.338	312	232.668	27.989
313	346.065	0.6001	314	324.529	-0.638	315	344.775	-0.296	316	338.030	0.0370
317	115.757	45.120	318	124.647	54.488	319	331.985	0.3701	320	131.475	59.715
321	20.2657	-0.300	322	29.2562	-0.278	323	23.9027	0.0149	324	49.2956	0.1095
325	180.414	14.055	326	203.926	13.330	327	179.574	15.287	328	195.905	40.248
329	189.013	39.046	330	136.555	26.672	331	124.107	20.652	332	117.587	17.169

333	221.580	31.938	334	229.761	29.016	335	144.877	33.526	336	156.226	35.127
337	195.074	34.944	338	204.919	33.689	339	142.756	26.819	340	197.703	34.078
341	198.162	34.065	342	203.709	33.309	343	209.014	32.716	344	161.604	33.789
345	197.488	30.913	346	200.106	30.602	347	205.873	31.003	348	203.169	31.986
349	202.401	32.400	350	196.213	31.725	351	159.327	30.371	352	223.132	25.337
353	229.458	24.139	354	234.594	22.445	355	233.594	23.501	356	225.305	21.006
357	234.024	18.348	358	222.488	22.278	359	240.338	16.306	360	204.683	26.328
361	211.438	25.392	362	228.788	21.329	363	233.159	19.884	364	227.019	22.308
365	236.443	21.568	366	239.405	20.755	367	236.073	16.952	368	226.009	21.072
369	229.920	19.815	370	246.651	14.096	371	222.187	22.990	372	208.172	23.029
373	242.006	54.611	374	137.512	22.851	375	144.277	25.502	376	145.949	26.374
377	162.641	27.772	378	124.292	15.915	379	166.420	29.146	380	127.104	18.132
381	131.427	19.725	382	134.827	17.588	383	120.268	11.429	384	177.835	26.471
385	120.352	11.916	386	139.235	19.302	387	172.147	26.381	388	167.698	26.375
389	153.964	24.728	390	170.867	27.510	391	176.846	28.055	392	203.811	25.044
393	162.443	22.669	394	164.961	24.057	395	120.475	9.6258	396	126.934	12.233
397	197.893	21.554	398	161.396	20.692	399	198.673	21.793	400	192.947	21.670
401	233.208	15.037	402	216.520	19.540	403	139.723	16.857	404	186.972	19.438
405	176.196	20.125	406	204.959	18.714	407	235.337	12.987	408	236.543	12.982
409	238.880	12.895	410	152.186	16.807	411	177.394	18.705	412	169.589	19.543
413	176.278	19.966	414	207.767	19.435	415	224.104	14.542	416	235.309	16.629
417	213.323	14.342	418	208.308	16.165	419	210.314	16.058	420	235.333	12.337
421	167.194	16.712	422	157.998	16.320	423	177.656	17.823	424	180.434	17.898
425	163.701	16.631	426	166.617	17.345	427	189.966	16.422	428	183.208	18.269
429	345.502	6.2461	430	119.332	11.206	431	26.8014	-10.21	432	128.536	11.987
433	151.758	13.983	434	130.783	11.085	435	176.932	1.8262	436	190.801	-2.003
437	190.383	1.5136	438	257.934	64.112	439	261.012	64.836	440	162.739	9.2651
441	222.847	57.139	442	122.795	18.567	443	116.312	32.762			

Table 1: Ring galaxy candidates identified automatically

| |

3.1 Comparison of the ring galaxy candidates to previous catalogues

The galaxies in the catalogue were compared to the catalogue of 275 polar ring galaxy candidates in SDSS (Moiseev et al. 2011). That catalogue showed 23 galaxies with a full ring that fit the morphology of the target galaxies shown in Table 1. The catalogue IDs of these galaxies are 7, 239, 240, 241, 243, 244, 245, 246, 249, 253, 254, 255, 256, 259, 260, 261, 263, 265, 267, 268, 270, 272, 274. Comparison to the galaxies in Table 1 shows that none of these galaxies were also included in Table 1. Therefore, Table 1 is clearly not a complete set of all SDSS galaxies with a full ring morphology, and many relevant galaxies with a full ring still exist in the SDSS database.

Comparing to the ring galaxies identified by Struck (2010), one (CGCG 222-022) of the 12 ring galaxies is included in this catalogue. The fact that just one galaxy is included in the catalogue shows that many more ring galaxies still exist in the SDSS database.

The list of automatically identified galaxies was also compared to the ring galaxies that were identified in SDSS by using citizen science (Buta 2017). The Buta (2017) catalogue contains 3,962 galaxies that volunteers identified manually by visually inspecting the images through an on-line web-based platform. From the 443 galaxies identified automatically, 104 are included in the Buta (2017) catalogue. The careful manual inspection process used in (Buta 2017) is clearly more accurate than any existing computer algorithm. However, the manual classification and annotation requires substantial labour, and therefore less than $3 \cdot 10^5$ galaxies were examined. The method described in this paper is automatic, and was applied to a much larger dataset of $\sim 2.6 \cdot 10^6$ galaxies, and therefore includes very many galaxies that were not examined by Buta (2017).

It can be expected that many of the objects listed in Table 1 have been identified previously and are part of existing catalogues. Table 2 shows the ring galaxy candidates that were also identified in previous studies.

3.2 Distribution and photometry of the ring galaxy candidates

As mentioned in Section 2, the galaxies in the catalogue described in Section 3 are galaxies detected among the subset of SDSS DR14 galaxies that have spectra. The galaxies included in the Buta (2017) catalogue are also galaxies with nuclear spectra. Because the galaxies are galaxies with spectra, their distribution in the sky is not uniform, but a distribution that corresponds to the spectroscopy survey of SDSS DR14. Therefore, the majority of the ring galaxy candidates are in the RA range of 120° - 240° . Figure 6 shows the distribution of the galaxies in Table 1 combined with the galaxies of the Buta (2017) catalogue by their redshift. The figure shows the number of galaxies, as well as their frequency among the galaxies with spectra in DR14 in the same redshift range. The Petrosian radius of all galaxies is larger than $5.5''$, which is large enough to allow the identification of the galaxy morphology (Timmis & Shamir 2017).

The graph shows that the frequency of the ring galaxy candidates in the catalogue starts to decline when the redshift is higher than 0.08. That can be explained by the less

detailed morphology of the imaged galaxies when the redshift gets higher, which does not allow clear identification of morphological details such as the presence of a full ring. The low frequency in the 0-0.02 range can be explained by a higher number of objects misidentified as galaxies by the SDSS pipeline, but are in fact not extra-galactic objects. In any case, in the redshift range of 0-0.02 the number of detected ring galaxy candidates is very small, and does not allow meaningful statistical analysis. Figure 7 shows the distribution of the ring galaxy candidates in Table 7. As the graph shows, the distribution is not substantially different from the distribution in the Buta (2017) catalogue.

Figure 8 shows the colour differences between the ring galaxy candidates including the galaxies of the Buta (2017) catalogue, and all other DR14 galaxies with spectra and Petrosian radius larger than $5.5''$. The graph shows that the u-g, r-i, and i-z declined with the increase in redshift for the galaxies identified as ring galaxies. That decline is in opposite trend to the other galaxies with spectra and Petrosian radius larger than $5.5''$. Also, the colour of the ring galaxy candidates changed in a more moderate manner with the redshift compared to the general galaxy population in SDSS DR14. That can be explained by the more morphologically homogeneous population in the set ring galaxy candidates, compared to the population of galaxies in SDSS. It should be noted that the majority of ring galaxy candidates are selected from the Galaxy Zoo 2 dataset, which are not a random selection of galaxies.

Figure 9 shows the colour differences between the ring galaxies in Table 1 and the other SDSS DR14 galaxies with spectra, and Petrosian radius larger than $5.5''$. The graphs show no significant differences between the colour of the ring galaxy candidates and the colour of other galaxies, with the exception of the u-g colour. The u-g of the ring galaxy candidates is lower in all redshift ranges compared to the u-g colour of the other galaxies in SDSS DR14 that have Petrosian radius larger than $5.5''$. The mean u-g of the ring galaxy candidates is 1.482 ± 0.018 , while the mean u-g of all other DR14 galaxies with Petrosian radius larger than $5.5''$ is 1.572 ± 0.0007 , and therefore the difference is statistically significant ($P < 0.001$). The difference in the blue colour can be explained by the fact that rings in star-forming galaxies have a larger visible contract, and therefore can be detected more easily in distant galaxies compared to the redder rings in the same redshift ranges. That can therefore increase the number of blue galaxies among ring galaxies compared to the general galaxy population.

The graphs also show substantial difference in all colours for galaxies in the redshift range of 0-0.02. That can be explained by stars identified by error as galaxies in the SDSS photometric pipeline. However, due to the small number of ring galaxies in that range no meaningful statistical analysis of the difference is possible. It should be noted that the galaxies in the Buta (2017) catalogue are bright and large objects selected by Galaxy Zoo 2, and are much larger than the objects in Table 1. The mean Petrosian radius (r band) of the galaxies in the (Buta 2017) is $\sim 19.28''$, while it is $\sim 9.67''$ for the galaxies in Table 1.



Figure 1. SDSS candidates of resonance ring galaxies.

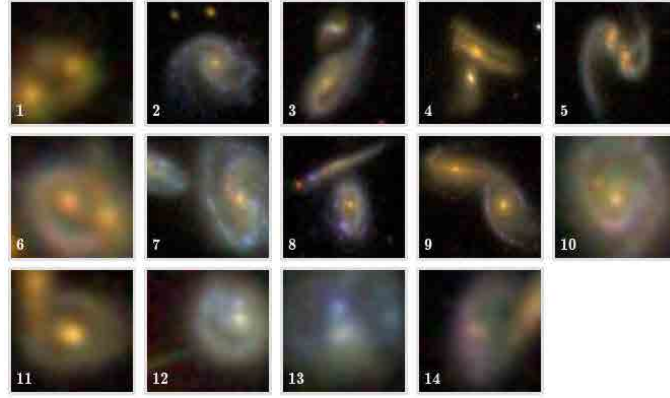


Figure 2. SDSS candidates of collisional ring galaxies.

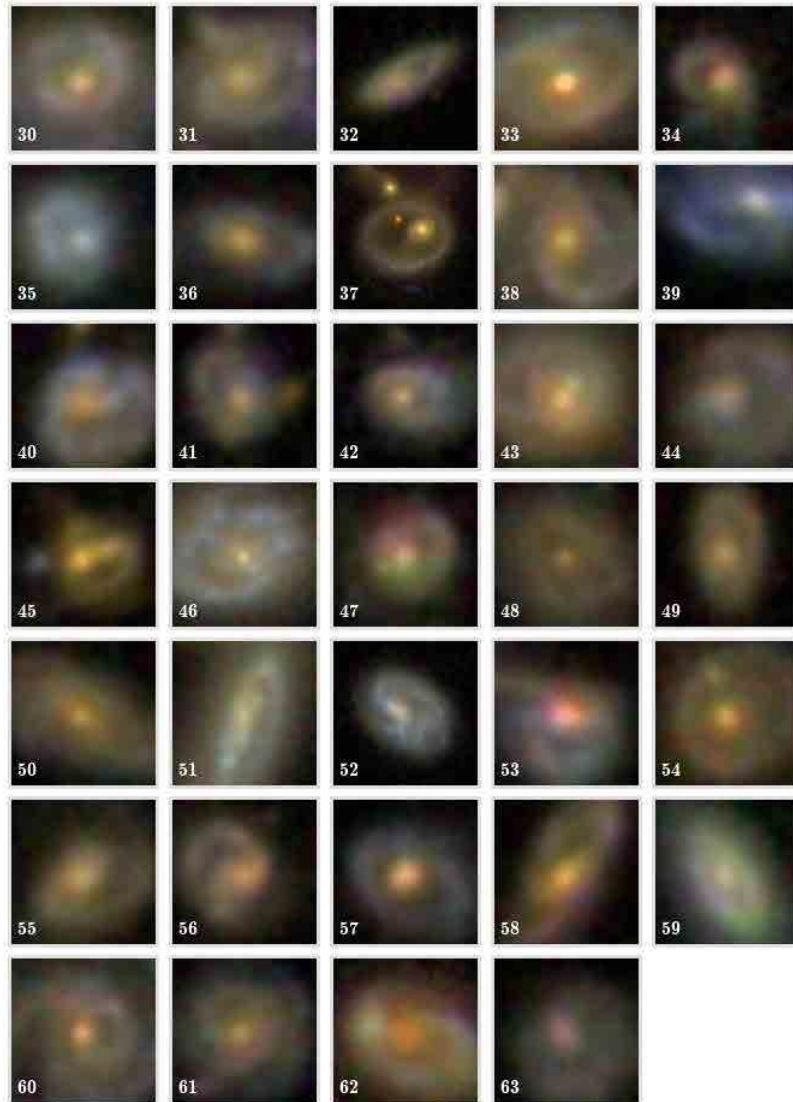


Figure 3. SDSS candidates of ring galaxies with off-centre nucleus.

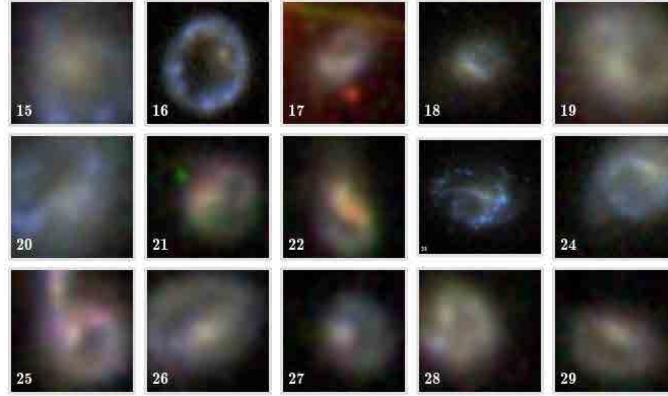


Figure 4. SDSS candidates of ring galaxies with no obvious nucleus inside the ring.

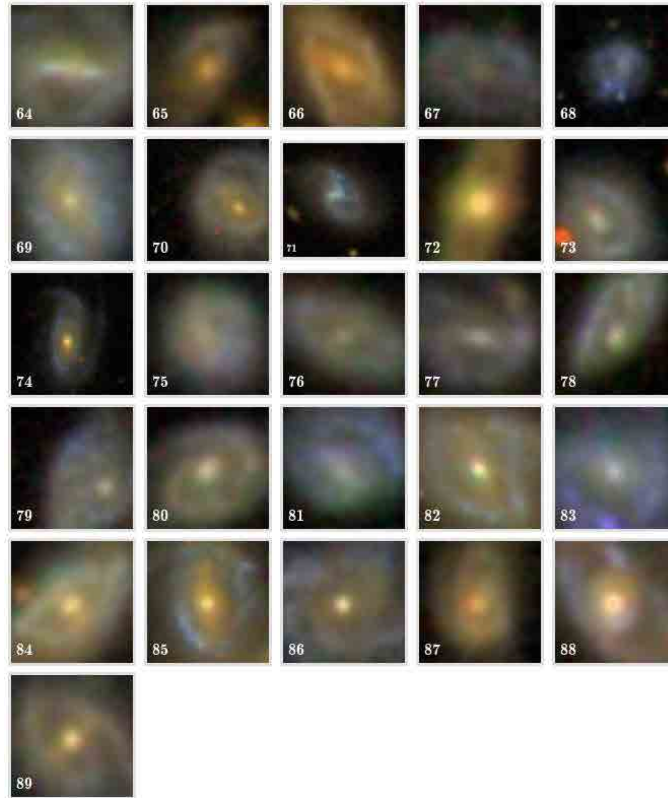


Figure 5. Other ring galaxy candidates in SDSS not included in Figures 1, 2, 4, and 3.

4 LIMITATIONS OF THE METHOD

The method used in this study aims at analyzing very large databases of galaxy images that might be too big to analyze manually, even when using crowdsourcing. That can only be done by automation. However, due to the very large databases of galaxy images, even a small false positive rate can lead to a very large number of false positive instances that becomes very difficult to handle manually. For instance, in the database used in this paper an algorithm with detection accuracy of 99% (which is normally considered extremely high in machine vision standards), would generate a dataset of $\sim 2.6 \cdot 10^5$ false positives. Therefore, a practical application of the method requires to minimize the false

positive rates. Since machine vision clearly does not meet the accuracy level of the human brain, achieving a low false positive rates require the sacrifice of some of the true positives.

As mentioned in Section 2, pixels below the threshold level of 50 were considered not sufficiently bright and were ignored. The JPEG threshold of 50 is in some cases high, and can lead to the exclusion of many ring galaxies such as the Hoag object (Schweizer et al. 1987), which has a clear but relatively dim ring compared to some other ring galaxies. However, lowering the threshold leads to a high number of false positives. For instance, Figure 10 shows examples of objects that are not ring galaxies, but the algorithm would have flagged them as rings if a lower graylevel threshold

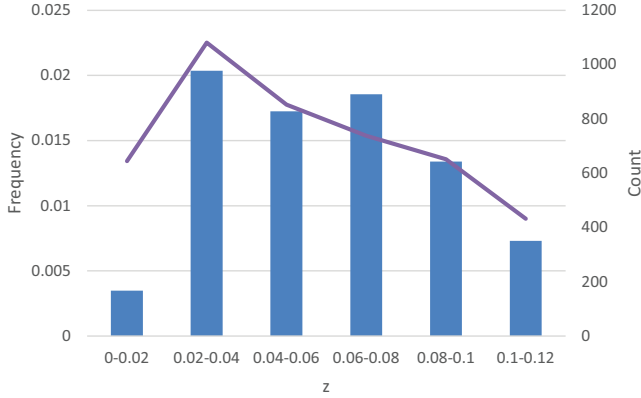


Figure 6. The number and frequency of the ring galaxy candidates in Table 1 combined with the galaxies of the Buta (2017) catalogue. The line shows the number of galaxies in each redshift range, and the bars show the frequency in the entire galaxy population.

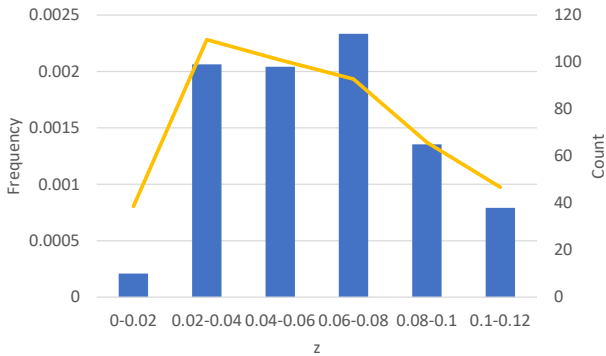


Figure 7. The number (line) and frequency (bars) of the ring galaxy candidates in Table 1 by redshift range.

would have been applied. Such objects are very common in the SDSS dataset, and many of them are flagged as galaxies by the SDSS photometric analysis pipeline. Since the method is designed to work with very large databases without the use of manual analysis, it sacrifices the detection of true positives, as even a small rate of false positives leads to an unmanageable output that requires a substantial step of manual analysis.

As discussed above, avoiding false positives is an important requirement, since due to the very large size of the database even a small false positive rate can make the method unusable. As a result, the detection method also has a high true negative rate, and many ring galaxies might not be detected by the method. To test the behavior of the methods and characterize the ring galaxies that it might fail to detect, ring galaxies from (Struck 2010) that were not detected by the method were examined. Figure 11 shows the first galaxies from the (Struck 2010) Galaxy Zoo sample that

were not detected by the method. The figure also shows the binary transformation of each image with different threshold levels.

For galaxies 2, 3, 5, and 6, a small background area surrounded by foreground pixels can be seen. However, these areas are smaller than 10% of the foreground, and therefore these galaxies are not flagged as ring candidates. In galaxies 1, 4, 6, and 8 part of the ring can be seen in the binary transform, but in none of the threshold levels the ring is complete in the sense that the background is completely surrounded by foreground pixels. For instance, in galaxy 4 the ring opens in the top right part of the galaxy. That happens because the ring is dimmer in that part, and the pixels in that part of the ring do not pass the threshold of the rest of the ring. In ring 6, the lower left part of the ring is dimmer than the rest of the ring, and therefore the ring cannot be detected by the method. In galaxy 3 the luminosity of the area inside the ring is not consistent, and therefore the ring is connected to the nucleus of the galaxy in the binary mask of the image. The same can also be seen in galaxy 5 and galaxy 2.

In galaxy 7, the ring is made of a slightly bluer colour, but the pixel intensity of the ring is not higher than the intensity of the pixels between the ring and the nucleus. Since the method first converts the pixels to grayscale, rings that are visible because they have different colour than the rest of the galaxy will not be detected.

These examples show that the method is mostly dependent on the consistency of the luminosity of the ring, as well as the part of the galaxy inside the ring. Rings that their luminosity varies might not be detected by the method because parts of the ring might not pass the luminosity threshold, leaving the ring in the binary mask open. The same is also for variation inside the ring. If the luminosity inside the ring varies, some parts inside the ring might pass the luminosity threshold and prevent the detection of the ring. Therefore, the method will not always detect ring galaxies that the luminosity of the ring or the parts inside it is not consistent across the different areas.

5 CONCLUSION

While ring galaxies are relatively rare, it can be assumed that the number of ring galaxies within a certain set of galaxies increases with the size of the dataset. The application of automatic identification can therefore allow the detection of such galaxies in very large databases, and is not limited by the availability of human resources that can scan the database manually. When much larger databases such as then Large Synoptic Survey Telescope (LSST) are collected, automatic detection will be able to identify many more ring galaxies.

The collection of ring galaxy candidates described in this paper is clearly not exhaustive, as evident by the differences between the galaxies in this catalogue and the galaxies in the catalogues of Moiseev et al. (2011), Buta (2017), or Struck (2010). Automatic analysis is still not as accurate as the human eye and brain, especially for the non-trivial problem of galaxy image analysis. However, automatic analysis has the clear advantage of analyzing data much faster than any human or group of humans. The purpose of the approach

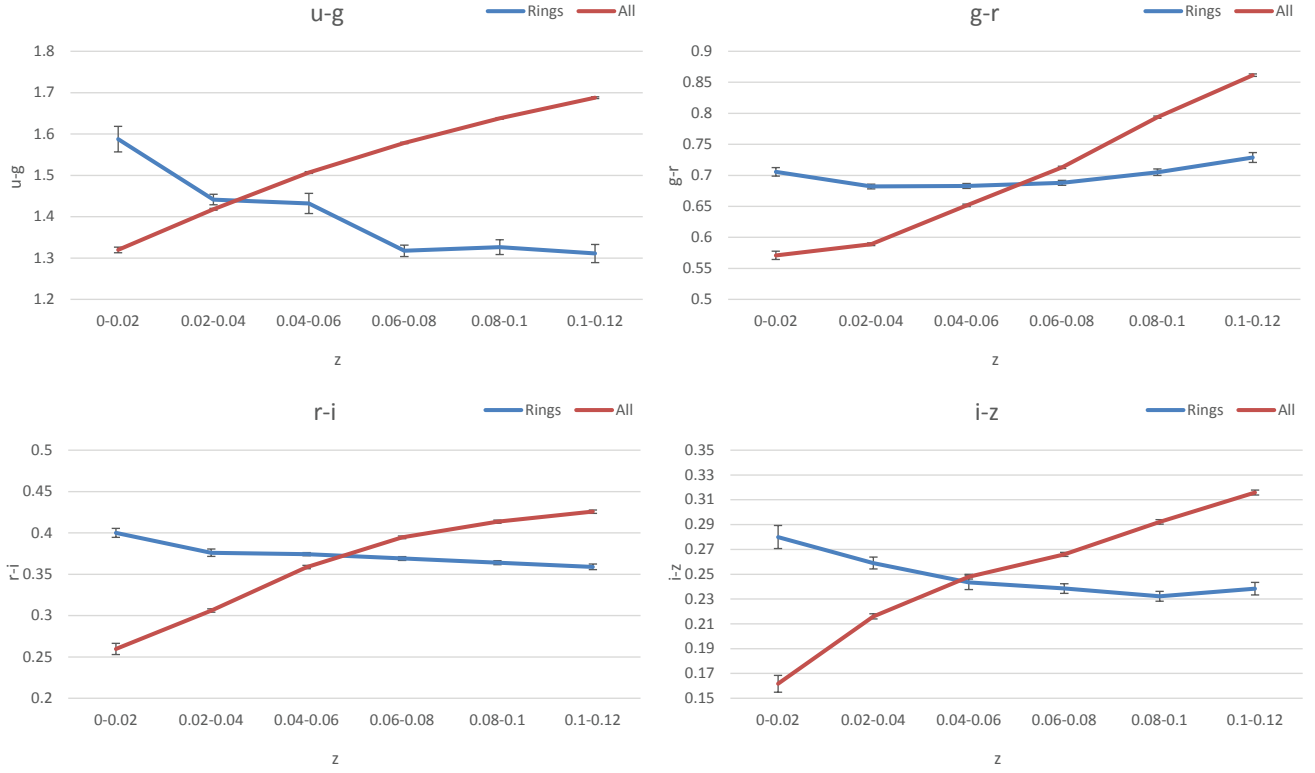


Figure 8. Colour differences between ring galaxy candidates and all galaxies.

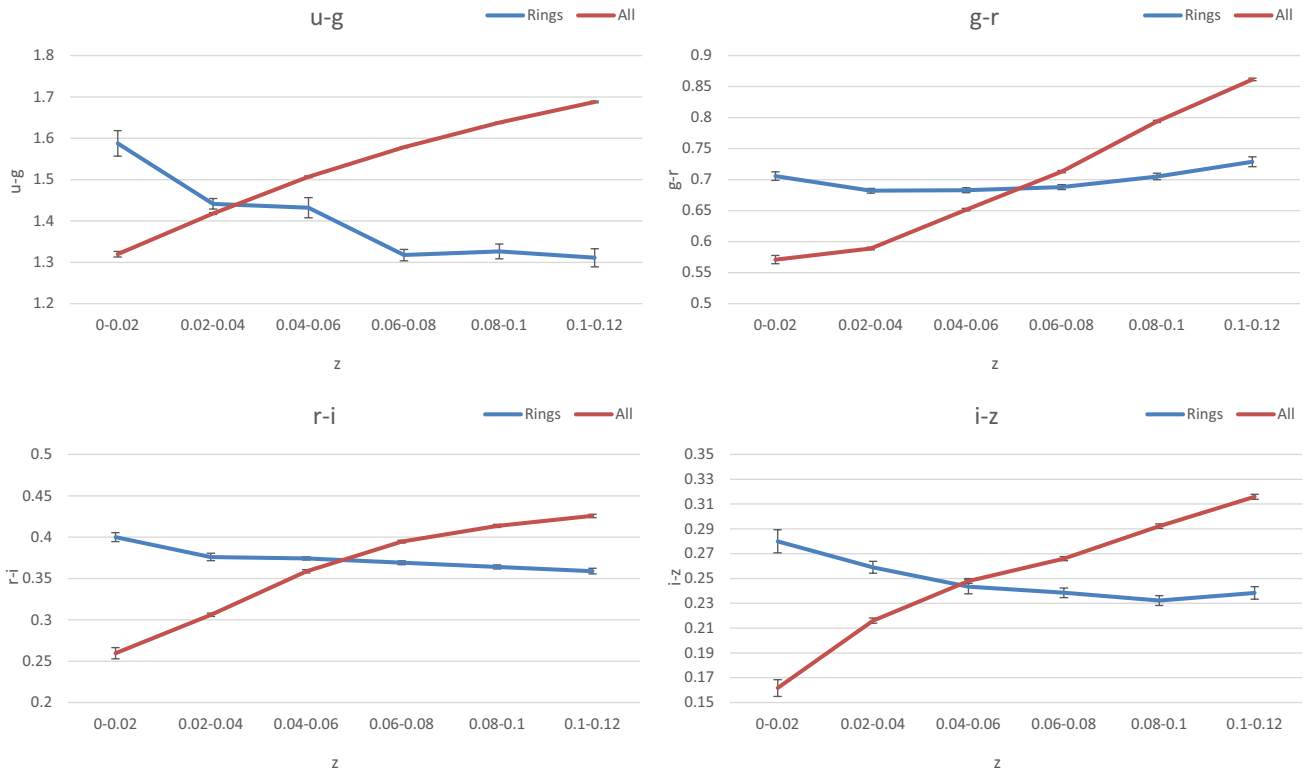


Figure 9. Colour differences between ring galaxy candidates of Table 1 and all galaxies with Petrosian radius larger than 5.5''.

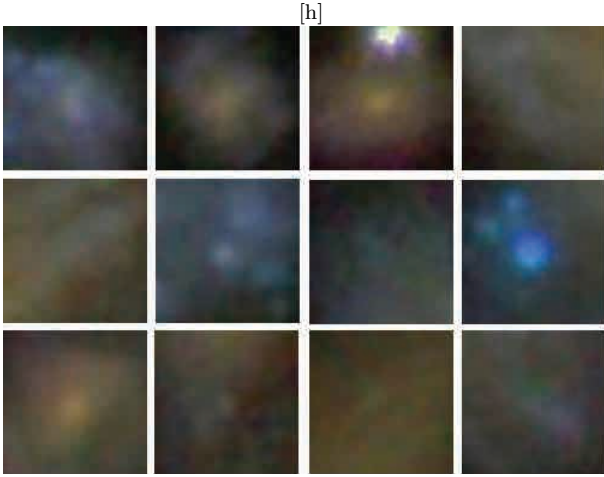


Figure 10. Example of galaxies that would have been flagged as ring galaxies below a graylevel threshold of 50.

described in this paper is to analyze very large databases of galaxies, under the assumption that even a small true positive rate can lead to large catalogues of ring galaxies.

Due to its higher sensitivity, the Buta (2017) catalogue of manually classified ring galaxies in SDSS already contains 104 of the galaxies identified in this study. But because the computer analysis method can scan much more galaxies with no cost of human labour, the vast majority of the galaxies identified in this study are not included in previous catalogues. It should be mentioned that the set of galaxies with spectra used as the initial database is not a completely random subset of SDSS galaxies, but selected by a certain algorithm (Reid et al. 2015).

While manual analysis of galaxy morphology has provided good collections of ring galaxies, the labour-intensive efforts required to compile such catalogues reduce the total number of galaxies that can be analyzed. As digital sky surveys are becoming increasingly more powerful, it is clear that automation will be required to analyze these databases and turn them into data products that enable scientific discoveries.

6 ACKNOWLEDGMENTS

This research was supported by NSF grants AST-1903823 and IIS-1546079. I would like to thank the anonymous reviewer for the insightful comments that helped to improve the paper. Funding for the SDSS and SDSS-II has been provided by the Alfred P. Sloan Foundation, the Participating Institutions, the National Science Foundation, the US Department of Energy, the National Aeronautics and Space Administration, the Japanese Monbukagakusho, the Max Planck Society, and the Higher Education Funding Council for England. The SDSS Web Site is <http://www.sdss.org/>. The SDSS is managed by the Astrophysical Research Consortium for the Participating Institutions. The Participating Institutions are the American Museum of Natural History, Astrophysical Institute Potsdam, University of Basel, University of Cambridge, Case Western Reserve University, University of Chicago, Drexel University, Fermilab, the Institute for Advanced Study, the Japan Participation Group,

Johns Hopkins University, the Joint Institute for Nuclear Astrophysics, the Kavli Institute for Particle Astrophysics and Cosmology, the Korean Scientist Group, the Chinese Academy of Sciences (LAMOST), Los Alamos National Laboratory, the Max Planck Institute for Astronomy (MPIA), the Max Planck Institute for Astrophysics (MPA), New Mexico State University, Ohio State University, University of Pittsburgh, University of Portsmouth, Princeton University, the United States Naval Observatory and the University of Washington.

REFERENCES

- Appleton P., Struck-Marcell C., 1996, *Fundamentals of Cosmic Physics*, 16, 18
- Arp H., 1966, *ApJS*, 14, 1
- Arp H. C., Madore B. F., 1988, *Contemporary Physics*, 29, 99
- Brosch N., 1985, *A&A*, 153, 199
- Buta R., 1995, *ApJS*, 96, 39
- Buta R., 2000, in , *Toward a New Millennium in Galaxy Morphology*. Springer, pp 79–99
- Buta R. J., 2017, *Monthly Notices of the Royal Astronomical Society*, 471, 4027
- Buta R. J., Combes F., 1996, *Fundamentals of Cosmic Physics*, 17, 95
- Buta R., Ryder S. D., Madsen G. J., Wesson K., Crocker D., Combes F., 2001, *ApJ*, 121, 225
- Dieleman S., Willett K. W., Dambre J., 2015, *Monthly notices of the royal astronomical society*, 450, 1441
- Few J. M., Madore B. F., 1986, *MNRAS*, 222, 673
- Finkelman I., Funes S. J. G., Brosch N., 2012, *MNRAS*, 422, 2386
- García-Ribera E., Pérez-Montero E., García-Benito R., Vilchez J., 2015, in *Highlights of Spanish Astrophysics VIII*. pp 372–372
- Hoag A. A., 1950, *AJ*, 55, 170
- Kuminski E., Shamir L., 2016, *ApJS*, 223, 20
- Macciò A. V., Moore B., Stadel J., 2005, *ApJL*, 636, L25
- Madore B. F., Nelson E., Petrillo K., 2009, *ApJS*, 181, 572
- Moiseev A. V., Smirnova K. I., Smirnova A. A., Reshetnikov V. P., 2011, *MNRAS*, 418, 244
- Reid B., et al., 2015, *MNRAS*, 455, 1553
- Reshetnikov V., Combes F., 2015, *MNRAS*, 447, 2287
- Reshetnikov V., Sotnikova N., 1997, *arXiv preprint astro-ph/9704047*
- Schweizer F., Ford Jr W. K., Jedrzejewski R., Giovanelli R., 1987, *ApJ*, 320, 454
- Shamir L., 2011a, *ApJ*, 736, 141
- Shamir L., 2011b, *Astrophysics Source Code Library*, ascl:1105.011
- Struck C., 2010, *Monthly Notices of the Royal Astronomical Society*, 403, 1516
- Theys J., Spiegel E., 1976, *ApJ*, 208, 650
- Timmis I., Shamir L., 2017, *ApJS*, 231, 2
- Whitmore B. C., Lucas R. A., McElroy D. B., Steiman-Cameron T. Y., Sackett P. D., Olling R. P., 1990, *AJ*, 100, 1489
- Willett K. W., et al., 2013, *Monthly Notices of the Royal Astronomical Society*, 435, 2835
- Zwicky F., Herzog E., 1968, *Catalogue of Galaxies and of Clusters of Galaxies*. Vol. 4, Caltech

This paper has been typeset from a $\text{\TeX}/\text{\LaTeX}$ file prepared by the author.

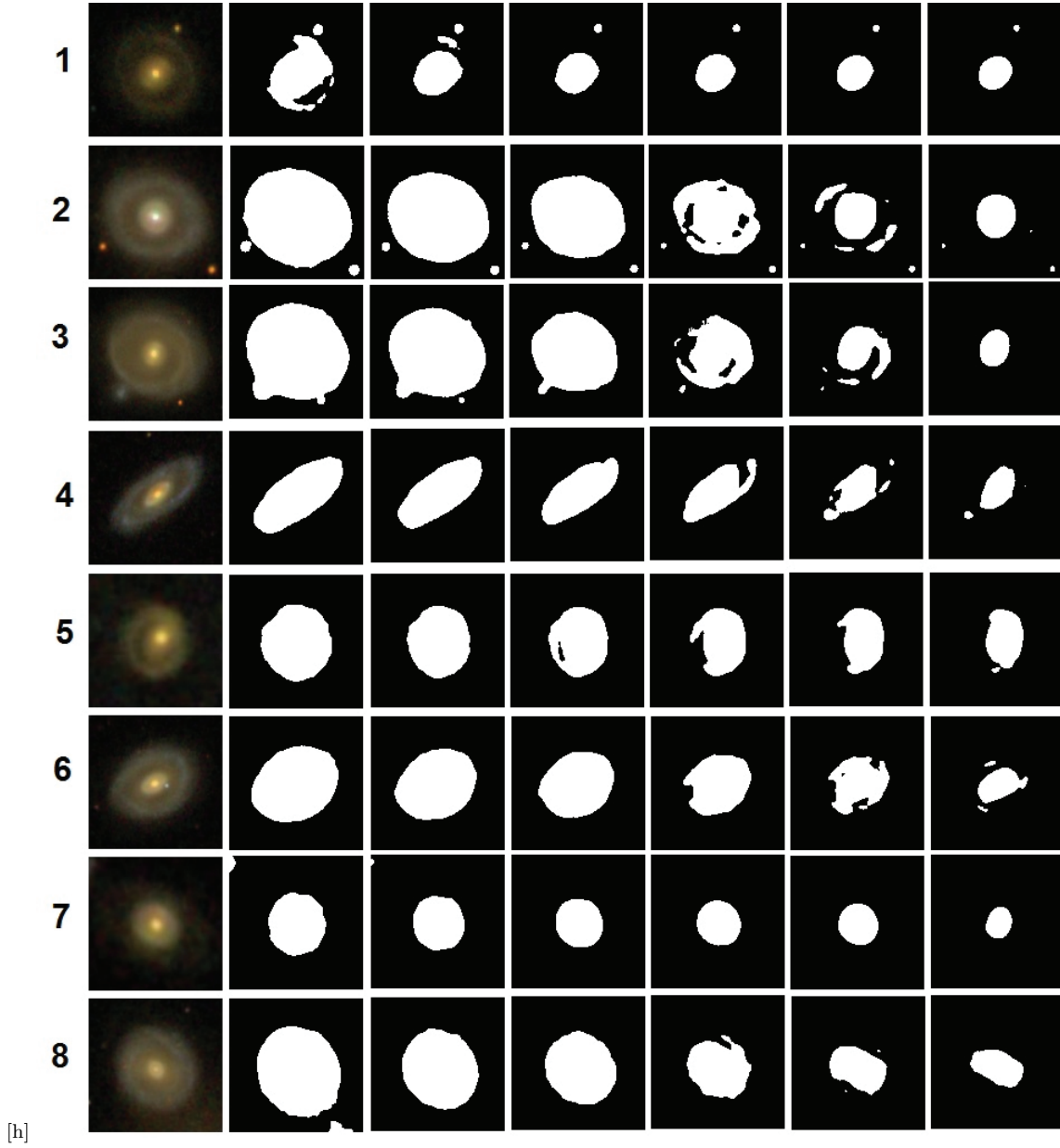


Figure 11. Ring galaxies from Struck (2010) catalogue that were not detected by the method, and the binary transformation with different thresholds.

#	Identifier	Ring Reference
4	MCG+07-19-002	
16	VII Zw 466	Zwicky & Herzog (1968)
23	MCG+05-23-004	
37	IIH4	Zwicky & Herzog (1968)
39	MCG+01-27-015	PGC 31038
60	IC 4074	
64	IC 1706	
78	NGC 7613	
82	NGC 4031	Buta (2017)
85	NGC 3754	
96	IC 1698	PGC 5261
101	MCG+08-15-041	Buta (2017)
110	IC 1010	
130	NGC 2740	Buta (2017)
140	NGC 5636	PGC 51785
141	IC 1007	PGC 51465
145	MCG+11-16-015	Buta (2017)
148	NGC 5876	Buta (2017)
153	NGC 6184	
154	UGC 10430	PGC 58385
155	UGC 10615	
181	MCG+10-16-093	
183	MCG+09-19-213	Buta (2017)
189	UGC 6109	
199	MCG+08-18-057	PGC 29124
203	MCG+08-22-038	
211	IC 699	Buta (2017)
216	MCG+11-15-044	
222	NGC 4566	
225	MCG+09-20-062	
228	UGC 10342	Buta (2017)
240	IC 2941	Buta (2017)
250	UGC 9691	
265	MCG+07-26-043	Buta (2017)
282	IC 3844	Buta (2017)
292	CGCG 222-022	Struck (2010)
295	NGC 5947	
308	MCG+04-39-016	
316	UGC 12068	PGC 69089
319	MCG+00-56-009	
323	MCG+00-05-013	PGC 5928
326	IC 901	
328	IC 4135	
337	MCG+06-29-011	
341	MCG+06-29-059	
349	UGC 8484	PGC 47369
359	UGC 10134	
360	MCG+05-32-048	
374	IC 2441C	
395	MCG+02-21-005	Buta (2017)
405	UGC 6719	
413	MCG+03-30-094	
424	MCG+03-31-015	
435	UGC 6769	Buta (2017)
440	NGC 3429	Buta (2017)

Table 2. Galaxies that are part of previous catalogues